Searching for Missing Binary Equiatomic Phases:

Oliynyk, Anton O.; Gaultois, Michael W.; Hermus, Martin; Morris, Andrew; Mar, Arthur; Brgoch, Jakoah

DOI:
10.1021/acs.inorgchem.8b01122
10.1021/acs.inorgchem.8b01122

Searching for Missing Binary Equiatomic Phases: Complex Crystal Chemistry in the Hf–In System

Anton O. Oliynyk,[†,§,*] Michael W. Gaultois,[‡] Martin Hermus,[†] Andrew J. Morris,[$] Arthur Mar,[§] and Jakoah Brgoch[†]

[†] *Department of Chemistry, University of Houston, Houston, TX 77204 USA*

[§] *Department of Chemistry, University of Alberta, Edmonton, AB T6G 2G2 Canada*

[‡] *Leverhulme Research Centre for Functional Materials Design, Materials Innovation Factory, Department of Chemistry, University of Liverpool, Liverpool L7 3NY, United Kingdom*

[$] *School of Metallurgy and Materials, University of Birmingham, Edgbaston, Birmingham, B15 2TT, UK*

Abstract

There remain 21 systems (out of over 3500 possible combinations of the elements) in which the existence of the simple binary equiatomic phases *AB* has not been established experimentally. Among these, the presumed binary phase HfIn is predicted to adopt the tetragonal CuAu-type structure (space group *P*4/*mmm*) by a recently developed machine-learning model and by structure optimization through global energy minimization. To test this prediction, the Hf–In system was investigated experimentally by reacting the elements in a 1:1 stoichiometry at 1070 K. Under the conditions investigated, the bulk and surface of the sample correspond to different crystalline phases, but have nearly the same equiatomic composition, as revealed by EDX analysis. The structure of the bulk sample, which was solved from powder X-ray diffraction data through simulated annealing, corresponds to the γ-brass (Cu_5Zn_8) type (space group $I\bar{4}3m$) with Hf and In atoms disordered over four sites. The structure of crystals selected from the surface, which was solved using single-crystal X-ray diffraction data, corresponds to the $CuPt_7$ type (space group $Fm\bar{3}m$) with Hf and In atoms partially disordered over three sites. The discrepancy between the predicted CuAu-type structure and the two experimentally refined crystal structures is reconciled through close inspection of structural relationships, which reveal that the γ-brass-type structure of the bulk HfIn phase is indeed derived through small distortions and defect formation within the CuAu-type structure.

1. Introduction

Binary equiatomic compounds *AB* have the simplest ratio of elements. As some of the most well studied compounds, they have played a critical role in developing fundamental understanding in chemistry. Indeed, key concepts in chemical bonding were first formulated in attempts to understand factors, such as atomic size, coordination preference, and electron count, that affect their formation.[1–3] These compounds also have many applications arising from their varied optical, thermal, and mechanical properties. Examples include CdSe and FeO pigments,[4,5] ZnTe infrared optical semiconductors,[6] CdTe and CuS photovoltaic materials;[6,7] BeO having high thermal conductivity,[8] TiC having low thermal conductivity;[9] and TaC, SiC, and *c*-BN high-hardness materials.[10–12] Given the long and exhaustive history of these *AB* compounds, it is natural to ask if there is anything else left to discover.

Out of 3547 possible combinations of elements, there remain only 21 systems in which experimental confirmation for the presence or absence of an *AB* compound has not been established.[13] It is not clear whether these compounds are missing because they do not exist, they are difficult to prepare, or perhaps simply nobody has tried to make them. There are also some inconsistent reports subject to revision; for example, the crystal structure of OsB[14,15] has been redetermined,[16,17] and the existence of CuF (in the ZnS-type structure[18]) has been challenged.[19] As part of ongoing efforts to apply machine-learning techniques to predict structures[20–22] and properties[23,24] of new compounds and materials using descriptors based only on the constituent elements, we have developed a model to classify the crystal structures of *AB* compounds.[13] These endeavours enabled by machine learning models have guided our synthetic attempts toward promising composition space and led to the discovery of RhCd,[13] the first new binary CsCl-type *AB* compound to be reported over the last ~15 years.[25] Like RhCd, many of

the missing *AB* compounds are composed of precious metals, whose high expense may have deterred experimentalists.

Before embarking on a search for the remaining missing compounds, it is prudent to decide on which compound to target on the premise that if it is to be useful in an eventual application, it should be composed of cheap and abundant starting materials. Plots of the estimated scarcity, Herfindahl-Hirschman index (HHI), and cost per gram for all possible *AB* combinations, including the missing ones, suggest that HfIn is an attractive target (Figure S1 in Supplementary Information).[26–28] Binary transition-metal indides have been poorly investigated until recently and indides in combination with early transition metals are still few.[29,30] Specifically, within the Hf–In system, the following binary phases have been previously reported: $Hf_{0.67}In_{1.33}$ (CuAu-type),[31] Hf_3In_4 (Ti_3In_4-type),[31,32] and Hf_2In_5 (Mn_2Hg_5-type).[33,34] No phase diagram or systematic studies of the Hf–In system have appeared.

We report here our attempts to prepare HfIn – and we evaluate the effectiveness of both machine-learning and first-principles approaches to predict its structure, determined experimentally through X-ray diffraction (XRD) analyses.

2. Experimental Section

2.1. Synthesis. Eight samples with the nominal composition HfIn were prepared following the same protocol to test for synthetic reproducibility. In a typical procedure, equiatomic mixtures of Hf (99.995%, Alfa-Aesar) and In powders (99.999%, Sigma-Aldrich) with a total mass of 0.5 g were pressed into pellets, which were arc-melted on a water-cooled copper hearth under an argon atmosphere in a Centorr arc furnace. The pellets were arc-melted twice to ensure homogeneity and the weight loss was <1%. The ingots were then annealed at

1070 K for one week in evacuated fused-silica tubes and then quenched in cold water. Additions of various fluxes (Al, Bi, Pn, Sn, In, Ga, NaCl–KCl) or vapour transport agents (I_2) were unsuccessful in yielding large single crystals.

The annealed ingots were crushed and examined on a JEOL JSM-6010LA scanning electron microscope (Figure 1a). Energy-dispersive X-ray (EDX) analysis on the interior surfaces of small ingot pieces gave an average composition of 51(2)% Hf and 49(2)% In, which agrees with the loaded composition. Closer examination of the exterior surfaces on these ingots also revealed the presence of small irregularly shaped single crystals that had a similar equiatomic composition of 50(2)% Hf and 50(2)% In (Figure 1b). Interestingly, the single crystals on the surface adopt a different structure from that of the bulk sample, as discussed below, and were thus characterized separately.

2.2. Characterization of Bulk Sample. Small pieces (20–50 μm) of the crushed HfIn ingots were initially selected under an optical microscope and evaluated on a Bruker PLATFORM single-crystal diffractometer equipped with a SMART APEX II CCD area detector and a graphite-monochromated Mo Kα radiation source (λ = 0.70296 Å). Out of more than 10 samples examined, all resulted in streaks instead of discrete spots observed on the CCD frames, indicating that these pieces were not single crystals but rather aggregates of randomly oriented polycrystallites, as verified when inspected under higher magnification in secondary and backscattered electron micrographs. When several CCD frames were combined into a single one, diffraction rings simulating a powder XRD pattern are evident (Figure 2a). In the absence of suitable single crystals, the bulk samples were ground into a fine powder and analyzed by powder XRD on a PANalytical Empyrean diffractometer with Cu Kα radiation (λ = 1.5418 Å). The powder XRD pattern agrees with the integrated CCD frames described above. The pattern

does not match with any existing Hf–In phase or any previously reported structure types based on a peak indexing search; it also does not correspond to the structure of the surface crystals. The structure was therefore determined from the powder data as discussed later.

2.3. Characterization of Surface Crystals. Small single crystals were selected from the surface on an uncrushed HfIn ingot and examined on a Bruker PLATFORM single-crystal diffractometer equipped with a SMART APEX II CCD area detector and a graphite-monochromated Mo Kα radiation source (λ = 0.70296 Å). Unlike the bulk sample, sharp diffraction spots were observed, confirming that these are indeed single crystals (Figure 2b). Intensity data were collected using ω scans at 8 different ϕ angles with a frame width of 0.3° and an exposure time of 30 s per frame. Structure solution and refinement were performed with use of the SHELXTL (version 6.12) program package.[35] Face-indexed numerical absorption corrections were applied. From the Laue symmetry, the cubic space group $Fm\bar{3}m$ was deduced. However, even casual inspection of the diffraction pattern (Figure 2b) reveals an unmistakable superstructure, which requires doubling the cubic unit cell parameter from 4.4 to 8.8 Å. Solution and refinement of the surface crystal structure are discussed later. Further data, in CIF format, have been sent to Fachinformationszentrum Karlsruhe, Abt. PROKA, 76344 Eggenstein-Leopoldshafen, Germany, as supplementary material No. CSD-434419 and can be obtained by contacting FIZ (quoting the article details and the corresponding CSD numbers).

2.4. Machine-Learning Model and First-Principles Calculations. To assist in the structure determination of the bulk sample, for which no suitable single crystals were available, initial guidance was sought from the machine-learning model previously developed to classify structures of binary *AB* compounds.[13] In this model, correlations are identified between independent variables (56 atomic descriptors such as size, position in periodic table, and physical

properties of the constituent elements of *AB* compounds) and dependent variables (7 classes corresponding to the most common structure types adopted by >97% of all *AB* compounds). Predictions for the most likely structure for HfIn were then made by evaluating probabilities for adopting each of the 7 structure types.

To complement the machine-learning predictions, first-principles DFT calculations were performed to suggest the lowest-energy structure of HfIn. This approach is unbiased and does not assume prior knowledge of previous structures. Because the number of potential structural candidates is large, it can be computationally expensive to consider all of them and it is desirable to reduce the number of candidates through structure search algorithms. A particle swarm optimization (PSO) algorithm was therefore implemented through the CALYPSO[36,37] code and coupled with the Vienna Ab initio Simulation Package (VASP)[38] to determine total energies. These calculations targeted the overall composition Hf_8In_8 with the number of formula units (Z) ranging from 2 to 4, yielding unit cell contents of 32, 48, and 64 atoms, respectively. In PSO, subsequent generations were developed based on the calculated enthalpies, in which the best (lowest enthalpy) 60% from the preceding generation were carried over and the remaining 40% were randomly generated. This search examined 800 possible crystal structures over 40 generations and was conducted three times to ensure that the global minimum was identified.

3. Results and Discussion

Arc-melting of equiatomic mixtures of Hf and In followed by annealing at 1070 K for one week resulted in the preparation of binary HfIn, as verified by EDX analyses, but in the form of two different phases, one which is representative of the bulk sample and one which appears as small crystals on the surface of the ingots.

3.1. Structure of Bulk Sample. Because single crystals of the bulk sample were unavailable, structure determination was attempted by analyzing the powder XRD pattern, which does not match any existing phases or common structure types. The most conventional way to analyze powder XRD patterns of an unknown structure is to apply automated procedures for peak indexing and search for high symmetry through programs such as TREOR,[39] DICVOL,[40] or FOX.[41] If all peaks in the range of 20–80° in 2θ are considered, with up to three peaks allowed to be attributed to impurity phases, these programs proposed the following possible unit cells, in order of increasing volume: a monoclinic unit cell (a = 4.39 Å, b = 3.05 Å, c = 4.33 Å, β = 99.7°) with three unassigned peaks, a tetragonal unit cell (a = 7.22 Å, c = 3.48 Å) with two unassigned peaks, and an orthorhombic unit cell (a = 14.45 Å, b = 14.58 Å, c = 3.06 Å) with one unassigned peak. Unfortunately, refinements based on these unit cells did not result in reasonable fits, so alternative methods were sought to solve the crystal structure.

According to a previously developed machine-learning model,[13] the tetragonal CuAu-type structure has the highest probability, among the seven most common structure types found for binary *AB* compounds, to be adopted by HfIn, even though it falls slightly below the decision barrier, by 2% in probability (Figure S2). In agreement with this proposal, a first-principles DFT calculation in which over 2400 possible structures were searched also established that the CuAu-type structure is the most energetically favourable one for HfIn. The DFT-optimized cell parameters are a = 3.1103 Å and c = 4.4982 Å. From the PSO algorithm, this structure has a favourable enthalpy change for the formation reaction, $\Delta H = [H(\mathrm{HfIn_{CuAu}}) - H(\mathrm{Hf_{hcp}}) - H(\mathrm{In_{tet}})]$, calculated to be –0.128 eV/atom. Moreover, it is dynamically stable, based on the phonon density of states calculated from the *ab initio* force constant method using PHONOPY[42] with 2 × 2 × 2 supercells and ±0.01 Å displacements. Altogether, these results argue for the favourable

formation of HfIn in the CuAu-type structure, at least in the size of the simulation cells considered.

Careful reasoning helped advance the investigation. In the experimental XRD pattern, the separation between the four major peaks and their relative intensities indicate a high-symmetry structure. The set of *d*-spacings of these intense peaks strongly suggests a similarity to the cubic CsCl-type structure with a cell parameter of a = ~3.5 Å. Given that the CuAu-type structure is a slightly tetragonally distorted variant of the CsCl-type structure, the proposals from the machine-learning and DFT models were not entirely misguided. The experimental powder XRD pattern for the bulk sample of HfIn was compared to a simulated one based on the CsCl-type structure (Figure 3), but the diffraction patterns still did not match. Close examination reveals that clusters of less intense peaks are also present, which can be fit to a unit cell tripled in all three dimensions. Analysis of systematic absences narrows down the possibilities to a cubic body-centred lattice with a cell parameter of a = ~10.5 Å and an atomic arrangement closely related to a 3 × 3 × 3 CsCl-type superstructure. After inspecting simulated diffraction patterns for entries satisfying these conditions in crystallographic databases (Pearson's Crystal Data),[30] we proposed that HfIn adopts a Cu_5Zn_8-type (γ-brass) structure, which crystallizes in space group $I\bar{4}3m$. The simulated pattern now agrees well with the experimental pattern (Figure 3). This initial assignment was difficult because HfIn has a much larger unit cell than typically found for other γ-brass structures, likely inhibiting the automated peak matching procedures to index the XRD pattern.

After the XRD pattern of bulk HfIn was fully indexed, it was fit using the TOPAS Academic software package.[43] In addition to space group $I\bar{4}3m$, other direct subgroups were considered: *P*222, *I*222, *Fmm*2, $I\bar{4}$, $I\bar{4}2m$, *P*23, and *I*23. Equivalent Pawley fits could be

obtained in all space groups, but clear systematic absences were observed in many cases. The best agreement with the experimental XRD pattern was obtained for $I\bar{4}3m$, the highest symmetry space group. Thus, this space group was accepted in an initial Pawley refinement to determine unit cell and peak shape parameters, after which simulated annealing was performed to locate atomic positions. Site mixing of Hf and In atoms must also be invoked to match intensities and account for some additional peak absences. Mixing of these two elements is common in related systems and has been observed for other compounds in the binary Hf–In system (*e.g.*, $Hf_{0.67}In_{1.33}$, and the solid solution between Hf_3In_4 and Hf_4In_5).

The final Rietveld refinement included all atomic positions, site occupancies, and isotropic displacement parameters. The displacement parameters generally converge to sensible values, although they are highly correlated to the site occupancies and scale factor. For the Hf2/In2 and Hf3/In3 sites, the refined displacement parameters were slightly too small, and later constrained to a lower limit of 0.01 $Å^2$, though this did not significantly influence the quality of the fit. Further, highly correlated and unreliable atomic displacement parameters are expected because of the limited *Q*-range obtainable using Cu radiation. Nevertheless, the refinement converged to give an agreement factor of R_{wp} = 4.23% and, more importantly, resulted in a good visual fit to the data (Figure 4). The refined composition is $Hf_{0.50(2)}In_{0.50(2)}$, consistent with the EDX analysis and the loaded composition. Barely perceptible impurity peaks in the XRD pattern probably result from slight oxidation, perhaps through exposure to air or moisture, as they are absent in freshly prepared samples. Further details of the Rietveld refinement are given in Table 1 and atomic coordinates for HfIn (Cu_5Zn_8-type) are listed in Table 2.

The γ-brass structure can be understood in terms of nesting four types of shells, each built by connecting atoms belonging to equivalent sites, as first described by Bradley and Jones.[44] An

inner tetrahedron of Hf4/In4 atoms is surrounded by an outer tetrahedron of Hf3/In3 atoms; these in turn are embedded within an octahedron of Hf2/In2 atoms and then within a cuboctahedron of Hf1/In1 atoms (Figure 5).

3.2. Structure of Surface Crystals. Small crystals found on the surface of the ingots were suitable for single-crystal X-ray diffraction analysis. The intensity data suggested cubic space group $Fm\bar{3}m$ with a prominent superstructure based on the Cu_3Au-type structure but with a doubled cell parameter of 8.8 Å. The structural model proposed by direct methods consisted of three sites at 4*a*, 4*b*, and 24*d*. Because the sizes of constituent elements in HfIn are nearly identical (with typical bond lengths of 3.02–3.06 Å for In–In, 3.02–3.06 Å for Hf–Hf, and 3.03 Å for Hf–In contacts), site assignments based on interatomic distances would be ambiguous. Several possibilities for the site occupations were considered, including ordered vs disordered models, and partial vs. full occupancies. These models were evaluated on the basis of the refinement results and the agreement of their compositions with the EDX analysis. The best agreement resulted from a partially ordered model consisting of half occupied Hf (4*a*), fully occupied In (4*b*), and disordered Hf/In sites (24*d*) (Figure 6). Further details of the data collection are given in Table 1 and atomic coordinates for HfIn ($CuPt_7$-type) are listed in Table 2.

The $CuPt_7$-type structure of these surface crystals of HfIn is a complex ordered superstructure of the Cu_3Au-type structure involving a symmetry-lowering *klassengleiche* transition of index 2.[45,46] This is a relatively unusual structure type adopted by less than a dozen compounds, generally of the composition AB_7, although a few representatives such as $Ce_{0.77}Pd_{7.23}$,[47] Cu_2Pt_6,[48] and $Pt_{6.65}Sb_{1.35}$[49] exhibiting site disorder are known.

3.3. Structural Relationships. At first glance, the two new phases of HfIn identified here, adopting the γ-brass (Cu_5Zn_8-type) structure for the bulk sample and the $CuPt_7$-type structure for the surface crystals, may appear to be unrelated. Because Hf and In are both relatively large atoms, these structures can be derived from two of the most basic archetypes best suited for packing equal sized spheres, to wit, the bcc (α-Fe-type) and fcc (Cu-type) structures adopted by many metallic elements (Figure 7). The γ-brass structure can be generated by taking the CsCl-type structure, the most commonly adopted by binary intermetallics *AB* and an ordered version of the bcc-type structure; forming defects and shifting the remaining atoms slightly toward these vacated sites; and then expanding to a 3 × 3 × 3 superstructure. As noted earlier, the CsCl-type structure is a more symmetric version of the tetragonally distorted CuAu-type structure, which was the one predicted by machine-learning and first-principles calculations.[13,50] The $CuPt_7$-type structure is generated by taking the Cu_3Au-type structure, an ordered version of the fcc-type structure; and then expanding to a 2 × 2 × 2 superstructure with a different ordering pattern. In the latter case, the equiatomic composition is achieved through appropriate site mixing of the Hf and In atoms.

Considerable disorder is present for both the γ-brass and $CuPt_7$-type forms of HfIn. In fact, the γ-brass-type structure is well known for its tendency to exhibit such disorder and is typically found with various combinations of d-block metals and group 13 or 14 metalloids.[51,52] The γ-brass-type structure does form in compounds containing In in combination with late transition metals (Cu,[53] Ag,[54] Au[55]), but HfIn is the first example containing a heavy early transition metal, and it has the largest unit cell known for all γ-brasses reported thus far. According to electron counting rules developed by Hume-Rothery, γ-brass-type structures are expected to have valence electron concentrations (vec) close to 21/13, or 1.6 e^-/atom.[56] If only

outer-shell electrons are considered, HfIn has a vec of 3.5 e^-/atom. The existence of a Hf-containing γ-brass opens up the possibility of preparing ternary variants through appropriate chemical substitutions.

3.4. Phase Equilibria. The observation of two forms of HfIn obtained in the same sample raises the question about their stability. The hypothesis is that the bulk sample (HfIn with γ-brass-type structure) represents the true thermodynamically stable phase and the surface crystals (HfIn with $CuPt_7$-type structure) correspond to a metastable phase. Arc-melted samples with varying Hf–In ratios were thus also prepared as described earlier and annealed at 800 °C. The powder XRD patterns of selected samples were examined and clearly established that HfIn with the γ-brass-type structure is the thermodynamically stable phase. It can be found in two-phase samples in equilibrium with either elemental Hf (Figure S3a) or Hf_3In_4 (Figure S3b). Despite their similar compositions, HfIn and Hf_3In_4 are distinct phases. On the other hand, Hf_3In_4 belongs to a solid solution extending to Hf_2In_5; both have the same tetragonal structure (space group *P*4/*mbm*), except that the ordered site distribution in Hf_2In_5 gives way to mixing of Hf and In atoms in one site in Hf_3In_4. On the In-rich side of Hf_2In_5, a two-phase sample reveals equilibrium with elemental In (Figure S3c).

An interesting observation is that the bulk HfIn powder sample undergoes vigorous reaction with water to produce a flammable gas, which is probably hydrogen (Figure S4a in Supporting Information). After the reaction product was dried at 100 °C for 1 day, the powder XRD pattern revealed that it contained a mixture of a Hf–In oxide of poor crystallinity and elemental In (Figure S4b in Supporting Information).

4. Conclusions

The apparent failure of machine-learning and first-principles approaches to correctly predict the structure of a heretofore unknown binary compound, HfIn, points to additional complexities exhibited by real compounds, namely disorder and site mixing, that were not considered in these models. Moreover, these are non-trivial to include in periodic models, necessitating searches involving large simulation cells, where even as DFT increases only $O(n^3)$ with number of electrons, the search space of candidate structures increases exponentially. Nevertheless, given the limited information available to these models, the prediction of a CuAu-type structure is the best possible one that can be made because the γ-brass-type structure of the observed thermodynamic phase HfIn can be derived from it. Indeed, γ-brasses are highly susceptible to site disorder. In fact, the suggestion of a CuAu-type structure was valuable in guiding the structure solution of the bulk sample of HfIn, for which no suitable single crystals were available. It is true that most equiatomic *AB* compounds usually adopt simple structures with relatively small unit cells (the most frequent being CsCl-, NaCl-, and ZnS-type structures), whose size is comparable to typical interatomic distances. However, this generalization belies the fact that even simple equiatomic compositions can give rise to extremely complex structures, sometimes with huge unit cells; for example, some SiC polymorphs can have unit cell volumes as large as 10,000 $Å^3$, compared to typical volumes of ~30 $Å^3$ for most *AB* structures. Future iterations of these predictive approaches will require careful consideration of disorder and the formation of solid solutions, which are common features of many intermetallic compounds.

Author Information

Corresponding Author

*E-mail: oliynyk@ualberta.ca (A. O. Oliynyk).

Notes

The authors declare no competing financial interest.

Acknowledgments

Financial support was provided by the Natural Sciences and Engineering Research Council of Canada through Discovery Grants. AOO gratefully acknowledges the Eby Nell McElrath Postdoctoral Fellowship at the University of Houston for financial support. MWG thanks the Leverhulme Trust for funding this research via the Leverhulme Research Centre for Functional Materials Design.

Supporting Information Available: X-ray crystallographic file in CIF format, estimated scarcity, HHI score, and cost of HfIn, summary of phase, probabilities predicted by machine-learning model for HfIn, analyses from powder XRD patterns. This material is available free of charge via the Internet at http://pubs.acs.org.

References

1. Abegg, R. Die Valenz und das periodische System. Versuch einer Theorie der Molekularverbindungen (Valency and the periodic system – Attempt at a theory of molecular compounds). *Z. Anorg. Allg. Chem* **1904**, *39* (1), 330–380.
2. Langmuir, I. The Arrangement of Electrons in Atoms and Molecules. *J. Am. Chem. Soc.* **1919**, *41* (6), 868–934.
3. Pauling, L. The principles determining the structure of complex ionic crystals. *J. Am. Chem. Soc.* **1929**, *51* (4), 1010–1026.
4. Hendry, E.; Koeberg, M.; Wang, F.; Zhang, H.; De Mello Donegá, C.; Vanmaekelbergh, D.; Bonn, M. Direct Observation of Electron-to-Hole Energy Transfer in CdSe Quantum Dots. *Phys. Rev. Lett.* **2006**, *96* (5), 057408-1–057408-4.
5. Cornell, R. M.; Schwertmann, U. The iron oxides: structure, properties, reactions, occurrences and uses. **2003**, Wiley VCH.
6. Amin, N.; Sopian, K.; Konagai, M. Numerical modeling of CdS/Cd Te and CdS/Cd Te/Zn Te solar cells as a function of Cd Te thickness. *Sol. Energy Mater. Sol. Cells* **2007**, *91* (13), 1202–1208.
7. Thulasi-Varma, C. V.; Rao, S. S.; Kumar C. S.; Gopi, C. V.; Durga, I. K.; Kim, S. K.; Punnoose, D.; Kim, H. J. Enhanced photovoltaic performance and time varied controllable growth of a CuS nanoplatelet structured thin film and its application as an efficient counter electrode for quantum dot-sensitized solar cells via a cost-effective chemical bath deposition. *Dalton Trans.* **2015**, *44*, 19330-19343.
8. Slack, G. A.; Austerman, S. B. Thermal Conductivity of BeO Single Crystals. *J. Appl. Phys.* **1971**, *42*, 4713–4717.
9. Morelli, D. T. Thermal conductivity and thermoelectric power of titanium carbide single crystals. *Phys. Rev. B* **1991**, *44*, 5453–5458.
10. Zhang, W.; Du, Y.; Peng, Y. Effect of TaC and NbC addition on the microstructure and hardness in graded cemented carbides: Simulations and experiments. *Ceram. Int.* **2016**, *42*, 428–435.
11. Arunkumar, K. N.; Krishnappa, G. B.; Kasthurirengan, S.; Vinay P. An Experimental Investigation on Hardness and Shear Behavior of Aluminum, Silicon Carbide, and Graphite Hybrid Composite with and without Cryogenic Treatment. *Mater. Today* **2018**, *5* (1), 916–921.
12. Weissmantel, S. Microstructure and Mechanical Properties of Pulsed Laser Deposited Boron Nitride Films. *Diamond Relat. Mater.* **1999**, *8* (2–5), 377–381.
13. Oliynyk, A. O.; Adutwum, L. A.; Harynuk, J. J.; Mar, A. Classifying Crystal Structures of Binary Compounds AB through Cluster Resolution Feature Selection and Support Vector Machine Analysis. *Chem. Mater.* **2016**, *28*, 6672–6681.
14. Aronsson, B.; Stenberg, E.; Åselius, J. Borides of Rhenium and the Platinum Metals. The Crystal Structure of Re_7B_3, ReB_3, Rh_7B_3, $RhB_{1.1}$ (approximate composition), $IrB_{1.1}$ (approximate composition) and PtB. *Acta Chem. Scand.* **1960**, *14*, 733–741.
15. Buddery, J. H.; Welch, A. J. E. Borides and Silicides of the Platinum Metals. *Nature* **1951**, *167*, 362.
16. Fokwa, B. P. T.; Misse, P. R. N.; Gillessen, M.; Dronskowski, R. Sn-flux syntheses, characterizations and bonding analyses of OsB and TiB_2. *J. Alloys Compd.* **2010**, *489*, 339–342.
17. Gu, Q. F.; Krauss, G.; Steurer, W. Transition metal borides: superhard versus ultra-incompressible. *Adv. Mater.* **2008**, *20*, 3620–3626.

18. Ebert, F.; Woitinek, H. Kristallstrukturen von Fluoriden. II. HgF, HgF_2, CuF und CuF_2. *Z. Anorg. Allg. Chem.* **1933**, *210*, 269–272.
19. Housecroft, C. E.; Sharpe, A. G. Inorganic Chemistry (3rd ed.). Prentice Hall. **2008**, 737–738.
20. Oliynyk, A. O.; Adutwum, L. A.; Rudyk, B. W.; Pisavadia, H.; Lotfi, S.; Hlukhyy, V.; Harynuk, J. J.; Mar, A.; Brgoch J. Disentangling Structural Confusion through Machine Learning: Structure Prediction and Polymorphism of Equiatomic Ternary Phases ABC. *J. Am. Chem. Soc.* **2017**, *139* (49), 17870–17881.
21. Oliynyk, A. O.; Mar, A. Discovery of Intermetallic Compounds from Traditional to Machine-Learning Approaches. *Acc. Chem. Res.* **2018**, *51* (1), 59–68.
22. Oliynyk, A. O.; Antono, E.; Sparks, T. D.; Ghadbeigi, L.; Gaultois, M. W.; Meredig, B.; Mar, A. High-Throughput Machine-Learning-Driven Synthesis of Full-Heusler Compounds. *Chem. Mater.* **2016**, *28* (20), 7324–7331.
23. Gaultois, M. W.; Oliynyk, A. O.; Mar, A.; Sparks, T. D.; Mulholland, G. J.; Meredig, B. Perspective: Web-based machine learning models for real-time screening of thermoelectric materials properties. APL Mater. **2016**, *4*, 053213-1–053213-11.
24. Sparks, T. D.; Gaultois, M. W.; Oliynyk, A. O.; Brgoch, J.; Meredig, B. Data mining our way to the next generation of thermoelectrics. *Scr. Mater.* **2016**, *111*, 10–15.
25. Gross, N.; Kotzyba, G.; Künnen, B.; Jeitschko, W. Binary Compounds of Rhodium and Zinc: RhZn, Rh_2Zn_{11}, and $RhZn_{13}$. *Z. Anorg. Allg. Chem.* **2001**, *627*, 155–163.
26. Gaultois, M. W.; Sparks, T. D.; Borg, C. K. H.; Seshadri, R.; Bonificio, W. D.; Clarke, D. R. Data-Driven Review of Thermoelectric Materials: Performance and Resource Considerations. Chem. Mater. 2013, 25, 2911-2920.
27. U.S. Department of Justice and the Federal Trade Commission. Horizontal merger guidelines, **2010**.
28. Tehrani, A. M.; Ghadbeigi, L.; Brgoch, J.; Sparks, T. D. Balancing Mechanical Properties and Sustainability in the Search for Superhard Materials. *Integr. Mater. Manuf. Innov.* **2017**, *6* (1), 1–8.
29. Villars, P.; Okamoto, H.; Cenzual K. (Eds.), ASM Alloy Phase Diagrams Database, ASM International, Materials Park, OH, 2016 (http://www.asminternational.org).
30. Pearson's Crystal Data: Crystal Structure Database for Inorganic Compounds (on DVD), Release 2015/16 ASM International®; Materials Park, OH, USA.
31. Raman, A.; Schubert, K. Über den Aufbau einiger zu $TiAl_3$ verwandter Legierungsreihen. II. Untersuchungen in einigen T-Al-Si- und T4...6-In-Systemen. *Z. Metallkd.* **1965**, *56*, 44–52.
32. Schubert, K.; Frank, K.; Gohle, R.; Maldonado, A.; Meissner, H. G.; Raman, A.; Rossteutscher, W.; Einige Strukturdaten metallischer Phasen. *Naturwissenschaften* **1963**, *50*, 41a.
33. Gulay, L. D.; Dubenskyy, V. P.; Zaremba, V. I.; Stepien Damm, J. The crystal structure of compound Hf_2In_5. *Visn. Lviv. Derzh. Univ., Ser. Khim.* **1999**, *38*, 3–5.
34. Pöttgen, R.; Dronskowski, R. Synthesis, Crystal Structure, Electronic Structure, and Properties of Hf_2In_5, a Metallic Hafnide with One-Dimensional Hf-Hf and Two-Dimensional In-In Bonding. *Chem. Eur. J.* **1996**, *2*, 800–804.
35. SHELXTL; Bruker AXS Inc.: Bruker AXS Inc.: Madison, WI, **2001**.
36. Wang, Y.; Lv, J.; Zhu, L.; Ma Y. Crystal Structure Prediction via Particle Swarm Optimization. *Phys. Rev. B* **2010**, *82*, 094116.

37. Wang, Y.; Lv, J.; Zhu, L.; Ma, Y. CALYPSO: A method for crystal structure prediction. *Comput. Phys. Commun.* **2012**, *183*, 2063–2070.
38. Kresse, G.; Joubert, D. From ultrasoft pseudopotentials to the projector augmented-wave method. *Phys. Rev. B* **1999**, *59*, 1758–1775.
39. Werner, P.-E.; Eriksson, L.; Westdahl, M. TREOR, a semi-exhaustive trial-and-error powder indexing program for all symmetries. *J. Appl. Cryst.* **1985**, *18*, 367–370.
40. Boultif, A.; Louer, D. Program for the Automatic Indexing of Powder Diffraction Patterns by the Successive Dichotomy Method. *J. Appl. Cryst.* **2004**, *37*, 724–731.
41. Favre-Nicolin, V.; Cerny, R. FOX, 'free objects for crystallography': a modular approach to ab initio structure determination from powder diffraction. *J. Appl. Cryst.* **2002**, *35*, 734–743.
42. Togo, A.; Oba, F.; Tanaka, I. First-principles calculations of the ferroelastic transition between rutile-type and $CaCl_2$-type SiO_2 at high pressures. *Phys. Rev. B: Condens. Matter* **2008**, *78*, 134106–134106.
43. Bruker AXS (2008): TOPAS V4: General profile and structure analysis software for powder diffraction data. - User's Manual, Bruker AXS, Karlsruhe, Germany.
44. Bradley, A. J.; Jones, P. An X-Ray Investigation of the Copper-Aluminium Alloys. *J. Inst. Met.* **1933**, *51*, 131–162.
45. Villars, P.; Cenzual, K.; Daams, J.; Gladyshevskii, R.; Shcherban, O.; Dubenskyy, V.; Melnichenko-Koblyuk, N.; Pavlyuk, O.; Stoiko, S.; Sysa, L. Structure Types. Part 1: Space Groups (230) Ia-3d -(219)-F43-c. Springer-Verlag Berlin Heidelberg, **2004**.
46. Pöttgen, R.; Johrendt, D. Intermetallics: synthesis, structure, function. Berlin : De Gruyter, **2014**.
47. Lipatov, A.; Gribanov, A. V.; Grytsiv, A. V.; Rogl, P.; Murashova, E. V.; Seropegin, Y. D.; Giester, G.; Kalmykov, K. The ternary system cerium-palladium-silicon. *J. Solid State Chem.* **2009**, *182*, 2497–2509.
48. Tang, Y. C. A cubic structure for the phase Pt_3Cu. *Acta Crystallogr.* **1951**, *4*, 377–378.
49. Durussel, P.; Feschotte, P. Les systèmes binaires Pd-Sb et Pt-Sb. *J. Alloys Compd.* **1991**, *176*, 173–181.
50. Levy, O.; Hart, G. L. W.; Curtarolo, S. Hafnium binary alloys from experiments and first principles. *Acta Mater.* **2010**, *58*, 2887–2897.
51. Gourdon, O.; Gout, D.; Williams, D. J.; Proffen, T.; Hobbs, S.; Miller, G. J. Atomic distributions in the gamma-brass structure of the Cu-Zn system: a structural and theoretical study. *Inorg Chem.* **2007**, *46* (1), 251–260.
52. Brandon, J. K.; Brizard, R. Y.; Chieh, P. C.; McMillan, R. K.; Pearson, W. B. New refinements of the [gamma] brass type structures Cu_5Zn_8, Cu_5Cd_8 and Fe_3Zn_{10} *Acta Cryst.* **1974**, *B30*, 1412–1417.
53. Che, G.C.; Ellner, M. Powder Crystal Data for the High-Temperature Phases Cu_4In, Cu_9In_4(h) and Cu_2In(h). *Powder Diffr.* **1992**, *7*, 107–108.
54. Hellner, E.; Laves, F. Kristallchemie des In und Ga in Legierungen mit einigen Übergangselementen (Ni, Pd, Pt, Cu, Ag und Au). *Z. Naturforsch. A* **1947**, *2*, 177–183.
55. Puselj, M.; Schubert, K. Kristallstrukturen von Au_9In_4(h) und Au_7In_3 *J. Less-Common Met.* **1975**, *41*, 33–44.
56. Hoistad, L. M.; Lee, S. The Hume-Rothery Electron Concentration Rules and Second Moment Scaling. *J. Am. Chem. Soc.* **1991**, *113*, 8216–8220.

Table 1. Crystallographic Data for HfIn Phases

formula	HfIn (bulk sample)	HfIn (surface crystals)
formula mass (amu)	293.31	293.31
space group	$I\bar{4}3m$ (No. 217)	$Fm\bar{3}m$ (No. 225)
a (Å)	10.5507(3)	8.827(5)
V (Å^3)	1174.5(1)	687.9(6)
Z	4	16
ρ_{calcd} (g cm^{-3})	10.777	11.329
T (K)	296	296
radiation	Cu Kα, λ = 1.5406 Å	Mo Kα, λ = 0.71073 Å
μ (mm^{-1})	76.97 (estimated)	73.11
2θ limits	8.00–150.00°	8.00–66.20°
refinement method	Rietveld	SHELXTL
no. of data collected	8676 data points	5551
no. of unique data	148 Bragg reflections	96 (R_{int} = 0.033) (52 with $F_o^2 > 2\sigma(F_o^2)$)
no. of variables	17	7
residuals [a]	R_B = 0.0127 R_p = 0.0321 R_{wp} = 0.0423	$R(F)$ ($F_o^2 > 2\sigma(F_o^2)$) = 0.017 $R_w(F_o^2)$ = 0.034

[a] $R_B = \sum |I_o - I_c| / \sum I_o$; $R_p = \sum |y_o - y_c| / \sum y_o$; $R_{wp} = [\sum [w(y_o - y_c)] / \sum w y_o^2]^{1/2}$;
$R(F) = \sum ||F_o| - |F_c|| / \sum |F_o|$; $R_w(F_o^2) = [\sum [w(F_o^2 - F_c^2)^2] / \sum w F_o^4]^{1/2}$,
$w^{-1} = [\sigma^2(F_o^2) + (Ap)^2 + Bp]$ where $p = [\max(F_o^2, 0) + 2F_c^2]/3$.

Table 2. Atomic Coordinates and Equivalent Isotropic Displacement Parameters for HfIn Phases

atom	Wyckoff position	occupancy	*x*	*y*	*z*	U_{eq} or U_{iso} (Å^2) [a]
HfIn (bulk powder): refined composition $Hf_{0.50(2)}In_{0.50(2)}$; EDX composition $Hf_{0.51(2)}In_{0.49(2)}$						
*M*1	24*g*	0.5(3) Hf, 0.5(3) In	0.1922(3)	0.1922(3)	0.5484(4)	0.048(2)
*M*2	12*e*	0.4(2) Hf, 0.6(2) In	0.6449(4)	0	0	0.01 [b]
*M*3	8*c*	0.6(3) Hf, 0.4(3) In	0.6015(3)	0.6015(3)	0.6015(3)	0.01 [b]
*M*4	8*c*	0.8(3) Hf, 0.2(3) In	0.8305(4)	0.8305(4)	0.8305(4)	0.021(2)
HfIn (surface crystals): refined composition $Hf_{0.53(1)}In_{0.47(1)}$; EDX composition $Hf_{0.52(2)}In_{0.48(2)}$						
Hf1	4*a*	0.541(6) Hf	0	0	0	0.006(1)
In1	4*b*	1.0 In	½	0	0	0.014(1)
*M*2	24*d*	0.58(2) Hf, 0.42(2) In	0	¼	¼	0.0095(4)

[a] U_{iso} applies to HfIn (bulk sample), for which Rietveld refinements were performed. U_{eq}, defined as one-third of the trace of the orthogonalized U_{ij} tensor, applies to HfIn (surface crystals).

[b] Lower limit constrained to 0.01 Å^2.

Table 3. Selected interatomic distances in the bulk HfIn structure ($I\bar{4}3m$).

Atom 1	Atom 2	Distance (Å)
M1	*M1*	3.199(2)
M1	*M2*	3.042(5)
M1	*M3*	3.129(6)
M1	*M4*	2.995(6)
M2	*M2*	3.058(9)
M2	*M3*	3.074(4)
M2	*M4*	3.199(3)
M3	*M3*	3.030(8)
M3	*M4*	3.034(5)
M4	*M4*	5.797(5)

Figure captions

Figure 1. SEM micrographs of HfIn samples. (a) A piece from a crushed ingot is not a single crystal, but an aggregate of polycrystallites. The composition determined by EDX at any of the positions indicated by a cross is equiatomic HfIn. (b) A surface crystal, not representative of the bulk sample, also has an equiatomic composition of HfIn. (The black circles are pieces of carbon tape on the surface.)

Figure 2. (a) Pieces (~20 μm) extracted from crushed ingots of HfIn exhibit diffraction rings, indicating that they are aggregates of polycrystallites. The integrated data on these CCD frames match with the powder XRD pattern of the bulk sample. (b) Crystals found on the surface of HfIn ingot, which are not representative of the bulk sample, exhibit sharp diffraction spots. Weak reflections indicative of a superstructure are easily seen.

Figure 3. The experimental powder X-ray diffractogram for bulk HfIn corresponds closely to the simulated pattern expected for HfIn in a Cu_5Zn_8-type crystal structure. Although all peaks present, heavy site disorder on all crystallographic sites is required to model the difference in observed intensities. It is clear that neither a hypothetical CsCl-type structure nor the $CuPt_7$-type structure adopted by the HfIn surface crystals have appropriate symmetry to describe the additional peaks present in the experimental XRD pattern of bulk HfIn.

Figure 4. A Rietveld fit to the X-ray diffractogram of bulk HfIn powder shows the experimental XRD pattern is well fit by the structural model presented here. Small impurity peaks in the XRD pattern probably result from slight oxidation, perhaps through exposure to air or moisture, as they are absent in freshly prepared samples.

Figure 5. The bulk sample of HfIn crystallizes in a γ-brass or Cu_5Zn_8-type crystal structure. The conventional description of the γ-brass structure consists of a subsequently nested polyhedral of increasing average volume: inner tetrahedron (IT), outer tetrahedron (OT), octahedron (OH), and cuboctahedron (CO)

Figure 6. The surface crystals of HfIn crystallize in a $CuPt_7$-type crystal structure.

Figure 7. Derivation of HfIn structures for bulk sample (Cu_5Zn_8-type) and surface crystals ($CuPt_7$-type). Each step down the hierarchy represents a lowering of symmetry. The final Cu_5Zn_8-type structure is created through defect formation in a 3×3×3 CsCl-type supercell.

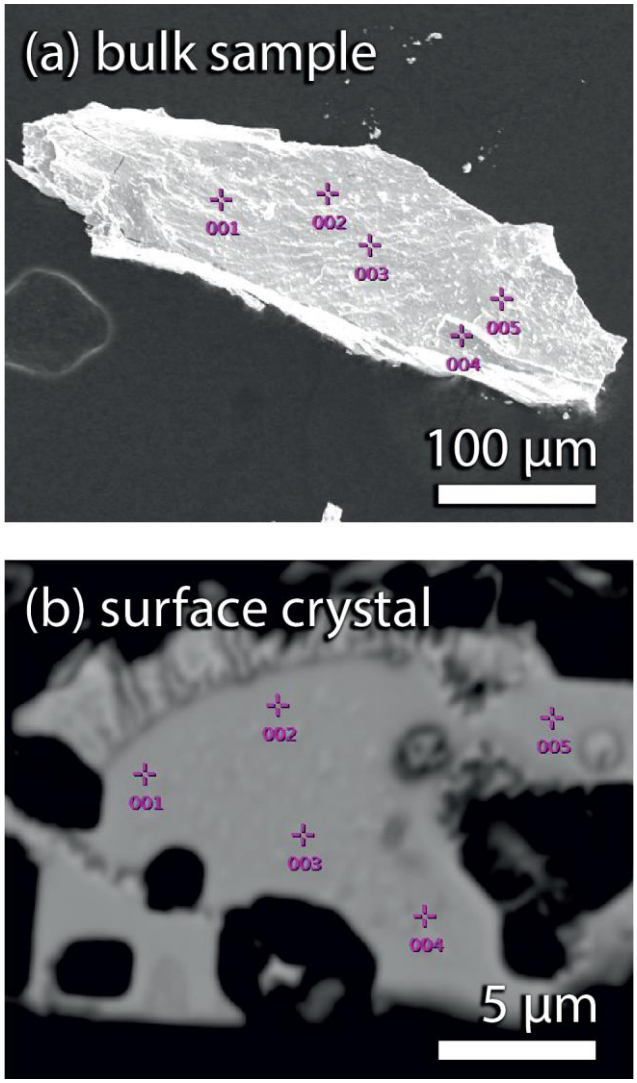

Figure 1. SEM micrographs of HfIn samples. (a) A piece from a crushed ingot is not a single crystal, but an aggregate of polycrystallites. The composition determined by EDX at any of the positions indicated by a cross is equiatomic HfIn. (b) A surface crystal, not representative of the bulk sample, also has an equiatomic composition of HfIn. (The black circles are pieces of carbon tape on the surface.)

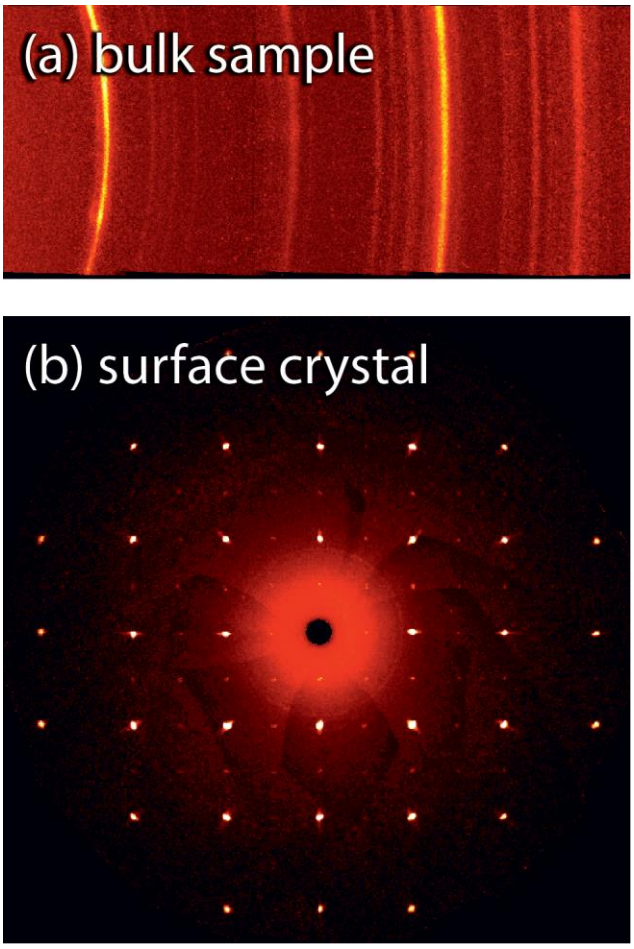

Figure 2. (a) Pieces (~20 μm) extracted from crushed ingots of HfIn exhibit diffraction rings, indicating that they are aggregates of polycrystallites. The integrated data on these CCD frames match with the powder XRD pattern of the bulk sample. (b) Crystals found on the surface of HfIn ingot, which are not representative of the bulk sample, exhibit sharp diffraction spots. Weak reflections indicative of a superstructure are easily seen.

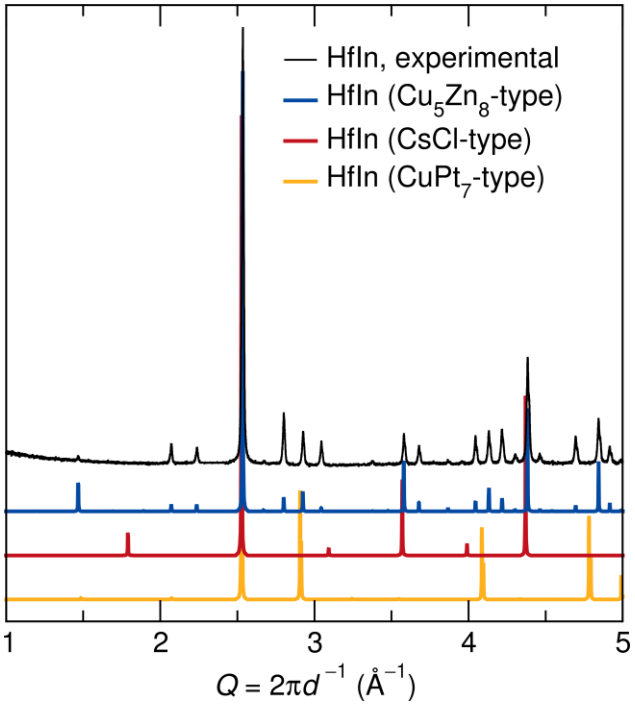

Figure 3. The experimental powder X-ray diffractogram for bulk HfIn corresponds closely to the simulated pattern expected for HfIn in a Cu_5Zn_8-type crystal structure. Although all peaks present, heavy site disorder on all crystallographic sites is required to model the difference in observed intensities. It is clear that neither a hypothetical CsCl-type structure nor the $CuPt_7$-type structure adopted by the HfIn surface crystals have appropriate symmetry to describe the additional peaks present in the experimental XRD pattern of bulk HfIn.

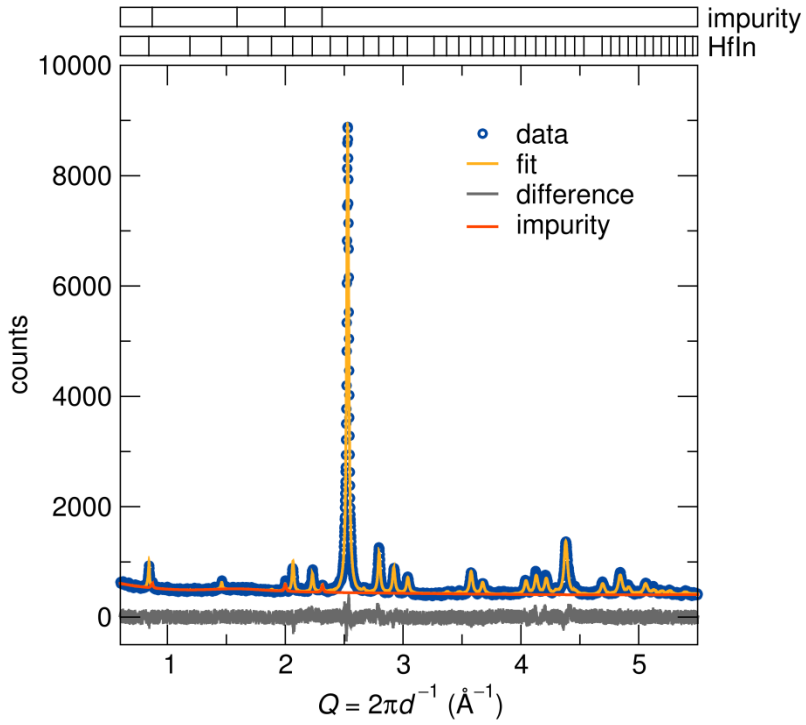

Figure 4. A Rietveld fit to the X-ray diffractogram of bulk HfIn powder shows the experimental XRD pattern is well fit by the structural model presented here. Small impurity peaks in the XRD pattern probably result from slight oxidation, perhaps through exposure to air or moisture, as they are absent in freshly prepared samples.

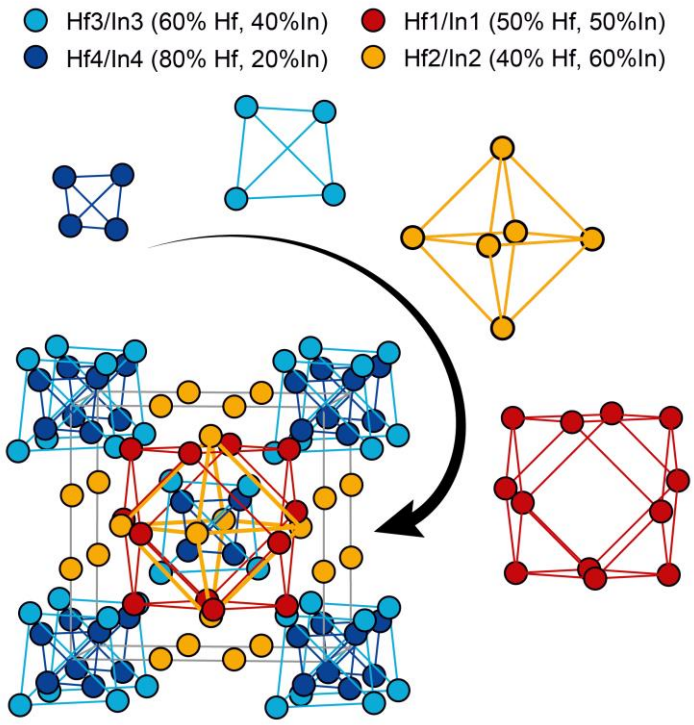

Figure 5. The bulk sample of HfIn crystallizes in a γ-brass or Cu_5Zn_8-type crystal structure. The conventional description of the γ-brass structure consists of a subsequently nested polyhedral of increasing average volume: inner tetrahedron (IT), outer tetrahedron (OT), octahedron (OH), and cuboctahedron (CO)

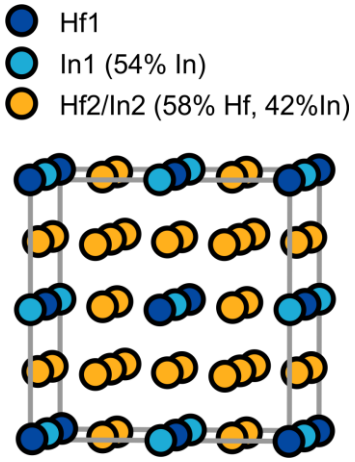

Figure 6. The surface crystals of HfIn crystallize in a $CuPt_7$-type crystal structure.

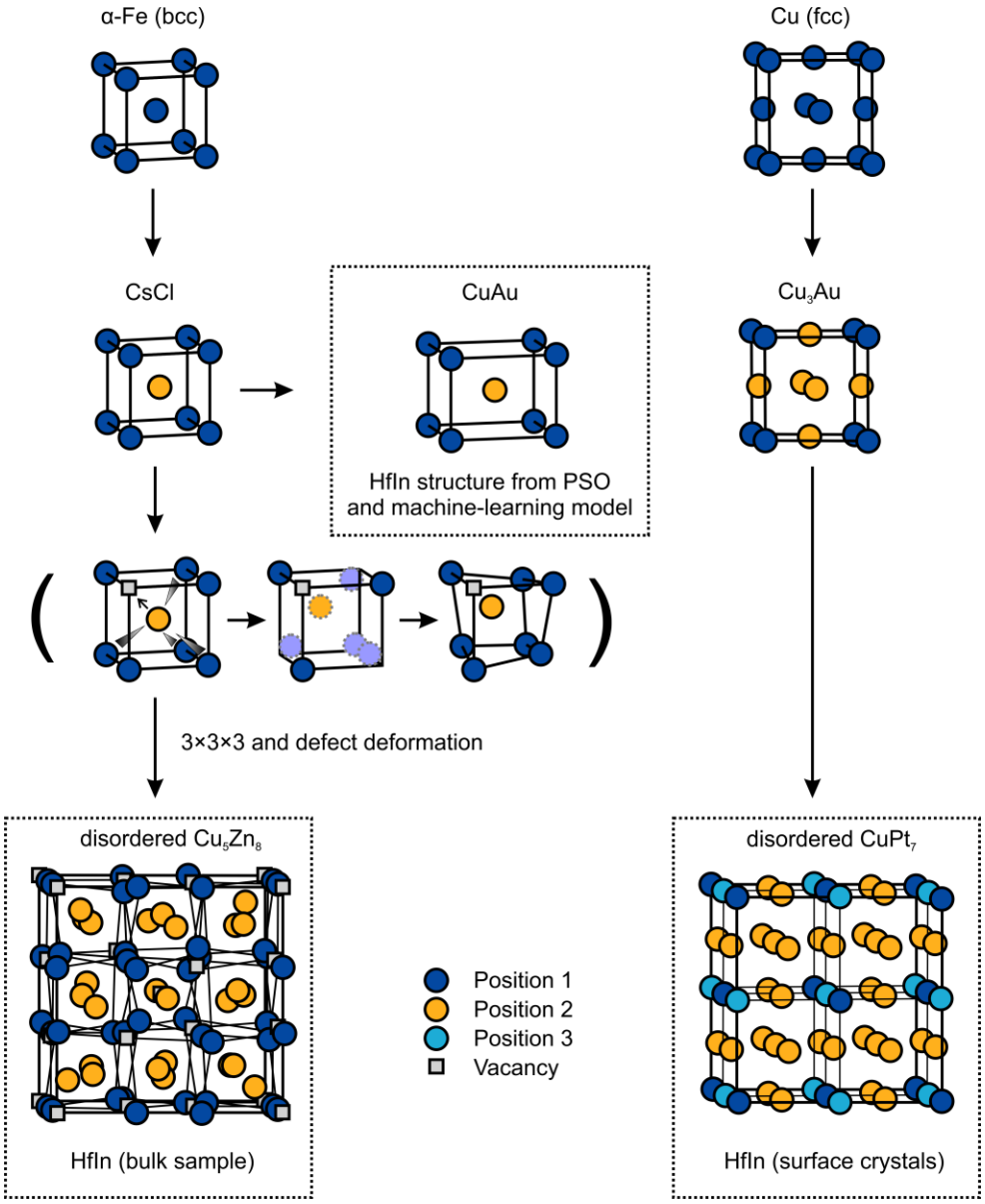

Figure 7. Derivation of HfIn structures for bulk sample (Cu_5Zn_8-type) and surface crystals ($CuPt_7$-type). Each step down the hierarchy represents a lowering of symmetry. The final Cu_5Zn_8-type structure is created through defect formation in a 3×3×3 CsCl-type supercell.

Table of Contents Synopsis

Anton O. Oliynyk,* Michael W. Gaultois, Martin Hermus, Andrew J. Morris, Arthur Mar, and Jakoah Brgoch *Inorg. Chem.* **2018**, *xx*, xxxx Searching for Missing Binary Equiatomic Phases: Complex Crystal Chemistry in the Hf–In System	Reaction between Hf and In in equiatomic stoichiometry results in γ-brass and $CuPt_7$-type structure.